



Research Paper

Inversion of on-tree peach firmness via high-fidelity fruit finite element models and sim-to-real deep transfer learning

Jiaqi Xiong ^a, Yilei Hu ^a, Xianbin Gu ^b, Ce Yang ^c, Di Cui ^{a,*}^a College of Biosystems Engineering and Food Science, Zhejiang University, Hangzhou, 310058, PR China^b Institute of Horticulture, Zhejiang Academy of Agricultural Sciences, Hangzhou, 310021, PR China^c Department of Bioproducts and Biosystems Engineering, University of Minnesota, Saint Paul, MN, 55108, USA

ARTICLE INFO

ABSTRACT

Keywords:

Acoustic vibration method
Finite element method
Deep transfer learning

Firmness is an important attribute of peaches related to texture and ripeness. The inversion of on-tree peach firmness contributes to monitoring fruit ripeness and determining the optimal harvest time for enhancing fruit quality. However, accurate inversion of fruit firmness is still challenging because of the limited number, range and distribution of training datasets. Therefore, an acoustic vibration method based on high-fidelity fruit finite element (FE) models and sim-to-real deep transfer learning was proposed for the inversion of the on-tree peach firmness with limited samples. Ten FE models of peaches comprising skin, flesh, pits and kernels were constructed to generate simulated vibration responses of on-tree peaches during fruit ripening. A 1D-Inception-SE network was established to extract features from the vibration responses to characterise peach firmness. To reduce the difference in feature distribution between the simulated dataset and the experimental dataset, a deep transfer learning method based on a domain adversarial neural network was introduced. The results indicated that the high-fidelity FE models of peaches were reliable for simulating the vibration behaviours of on-tree peaches during fruit ripening. The proposed deep transfer learning method raised the R^2 of the test set from 0.79 to 0.83. Compared to the 1D-Inception-SE model with 320 experimental samples, the deep transfer learning model with both simulated data and 160 experimental samples achieves superior performance while requiring only half the number of experimental samples. The results demonstrated that the proposed method could efficiently and effectively improve the firmness inversion accuracy for on-tree peaches by measuring limited samples.

Nomenclature

(continued)

A	the cross-sectional area of the sample	f_t	extracting features from x_t using G_f
C	the number of vibration signals	G_d	the domain classifier
CNNs	convolutional neural networks	G_f	the feature extractor
D	the deformation of the object	G_p	the predictor
DAFB	days after full bloom	GRL	gradient reversal layer
DANN	domain-adversarial neural network	g	An intermediate transformation function
$\mathcal{D}_{\text{source}}$	the source domain	L	the length of the vibration signal
$\mathcal{D}_{\text{target}}$	the target domain	LDV	laser Doppler vibrometer
E	the elastic modulus of the object	ΔL	the deformation of the sample
F	the compressive force	MSE	mean squared error
FE	finite element	N	the input channel number
F_{ex}	the function of the excitation operation	N_s	the size of the source dataset
FFT	fast Fourier transform	N_t	the size of the target dataset
f	domain discriminator input	PSD	Power spectral density
f_s	extracting features from x_s using G_f	R^2	coefficient of determination
		R^C	a real number space

(continued on next column)

(continued on next page)

* Corresponding author. 866 Yuhangtang Rd., Hangzhou, 310058, Zhejiang, PR China.

E-mail address: dicui@zju.edu.cn (D. Cui).

(continued)

R_L	the maximum radii of curvature of the contact points on the lower surface
R'_L	the minimum radii of curvature of the contact points on the lower surface
RMSE	root mean square error
R_U	the maximum radii of curvature of the contact points on the upper surface
R'_U	the minimum radii of curvature of the contact points on the upper surface
RUL	remaining useful life
r	reduction ratio
SE	squeeze-and-excitation
s	source
t	target
t-SNE	t-Distributed stochastic neighbor embedding
$u_c(i)$	the value of the i -th feature of the c -th vibration signal.
W	the weight matrix
W_1	the weight matrices of a fully connected layers
W_2	the weight matrices of the other connected layers
x_s	the input feature from the source domain
x_t	the input feature from the target domain
y_s	the corresponding label of x_s
y_t	the corresponding label of x_t
Z	the real-valued sequence obtained through global average pooling
Z_n	the n -th element of Z
δ	the ReLU activation function
\mathcal{L}	total loss
\mathcal{L}_d	the domain classifier loss
$\nabla \mathcal{L}$	the gradient of the total loss
∇L_d	the gradient of the domain loss
\mathcal{L}_p	the firmness predictor loss
λ	a weight parameter
σ	the sigmoid function
η	the learning rate
θ_d	the parameters of the domain classifier
θ_f	the parameters of the feature extractor
θ_p	the parameters of the predictor

1. Introduction

Peaches (*Prunus persica* L.) are one of the most popular fruits for consumers since they are delicious and contain a variety of vitamins, minerals and organic acids (Zhang et al., 2020). As a key quality indicator of peaches, firmness is significantly correlated with their mouth-feel, ripeness and storability (Nouri & Abdanan Mehdizadeh, 2024). The demand for firmness measurement spans the entire peach industry (Gonçalves et al., 2016). The peaches harvested within a specific firmness threshold usually show greater resistance to mechanical damage, possess longer shelf life, and exhibit better sensory performance after complete softening (Ma et al., 2024). Hence, the firmness of peaches at preharvest is crucial for determining the optimum picking time of peaches.

Fruit is a highly complex multi-degree-of-freedom biological system. The firmness of fruit, which is a critical mechanical property, can be characterised by its elastic modulus. Traditional measurements of firmness have typically relied on texture analyzers and penetrometers. However, these methods are both destructive and labour-intensive. An alternative approach has shown impressive potential in non-destructive and effective detection of fruit firmness by analysing the vibration responses of fruits to an excitation force (Zhang et al., 2018). This method, known as the acoustic vibration method, has been used in controlled environments during postharvest processing to assess fruit firmness (Diezma-Iglesias et al., 2006; Ding et al., 2022; Zhang et al., 2021). Nevertheless, the accuracy of fruit firmness assessment via the acoustic vibration method still requires improvement.

The commonly used method for fruit firmness inversion involves first converting the vibration response of the fruit from the time domain to the frequency domain using the Fast Fourier Transform (FFT), then extracting feature parameters (such as resonance frequency, amplitude and phase shift), calculating vibration indicators (such as elastic index and stiffness coefficient), and finally establishing the firmness inversion model using linear regression or classical machine learning algorithms (Kondo et al., 2014; Landahl & Terry, 2020). Although this method has a clear mechanism and is easy to deploy, its inversion accuracy for fruit

firmness is relatively low. With the rapid development of deep learning technologies, especially the emergence of convolutional neural networks (CNNs), deep learning-based approaches have been adopted for the inversion of fruit firmness (Lin et al., 2023). Wang et al. (2022) proposed an improved 1D-CNN with multiscale convolution for unsupervised extraction of vibration features from the vibration responses of peaches and inversion of fruit firmness, resulting in a 6 % increase in accuracy. The quality and quantity of samples significantly impact the performance of deep learning-based approaches. Sufficient and representative samples facilitate better learning of data characteristics (Castiglioni et al., 2021). However, collecting a large number of high-quality samples not only increases the investment of labour, materials and funds but also increases various biases caused by many experiments.

Numerical simulation provides an alternative way to enlarge the dataset. Researchers have obtained a large amount of simulated data by simulating the vibration response of objects under different loads. This approach has been successfully applied in fault monitoring in the industrial field (Lou et al., 2023). Due to the structural characteristics and material properties of fruits are more complex than those of mechanical components, prior finite element (FE) models of fruits have often simplified the shape, internal structure, or material properties of fruits (Abbaszadeh et al., 2014; Pereira et al., 2023). This has led to considerable differences between the simulated data derived from fruit FE models and experimental data (Rashvand et al., 2022; Zulkifli et al., 2020), making it difficult to use the simulated data for establishing fruit quality inversion models. As a result, fruit vibration data obtained through simulation have not yet been used to enlarge the dataset. Although some scholars have tried to establish high-fidelity FE models of agricultural objects to improve the similarity between simulated and experimental data (Melo et al., 2024), a gap still exists between them.

Taking inspiration from human learning mechanisms, transfer learning aims to reuse knowledge learned from a related field (source domain) to enhance model performance or reduce the required sample size in the target domain (Lu et al., 2015). To minimise the discrepancy between the two domains, domain adaptation is commonly used in transfer learning (Zhuang et al., 2021), which can mitigate the gap between the source domain and the target domain. The domain-adversarial neural network (DANN) (Ganin et al., 2017) integrates the concept of adversarial learning with transfer learning approaches and aims to extract domain-invariant features, enabling the target domain dataset to adapt to the model established with the source domain dataset. Currently, the method of transferring simulated vibration data from FE models to experimental data for constructing detection models has been predominantly utilized in the fields of civil engineering and mechanical engineering, such as mechanical fault detection (Xu, 2024) and bridge health monitoring (Luo et al., 2024). To the best of our knowledge, this method has not yet been used to transfer simulation data from FE models of agricultural products to experimental data, mainly due to the insufficient accuracy of the prior models.

The general objective of this study is to propose an efficient approach for accurate inversion of the firmness of on-tree peaches with limited samples. The specific objectives are as follows: 1) to construct high-fidelity FE models of peaches to simulate the vibration responses of on-tree peaches and 2) to propose an effective method for transferring the features derived from simulated vibration responses to experimental ones, thereby achieving accurate firmness inversion for on-tree peaches with fewer samples.

2. Materials and methods

2.1. Plant materials

The peach cultivar Dongxi Xiaolian (*Prunus persica* (L.) Batsch) was chosen as the sample in this study. The peaches were grown in the orchard of the Zhejiang Academy of Agricultural Sciences located in

Jiaxing, Zhejiang Province, China. A total of 400 peaches at 103–111 days after full bloom (DAFB) were collected in 2022 and 2023, of which 320 peaches were used to measure their vibration responses while on the tree and fruit firmness in the laboratory (Section 2.2.1). Ten peaches at different DAFBs were subjected to both 3D scanning and mechanical property tests in the laboratory (Section 2.2.2) to establish high-fidelity FE models of the peaches (Section 2.3). The additional 70 peaches were used solely for mechanical property testing to acquire the range of material parameters during peach ripening for the simulation process. To reduce the impact of softening after harvest on peach firmness, all the samples were transported to the laboratory immediately by a car, after firmness measurements, 3D scanning and mechanical property tests were carried out within 24 h.

2.2. Experimental data collection

2.2.1. Vibration and firmness measurement

The device for measuring the acoustic vibration response of on-tree peaches consists of an excitation unit and a vibration measurement unit (Fig. 1). The excitation unit includes an air compressor (E8L, Zhejiang Jonway Machinery & Electric Manufacture Co., Ltd., China), a pressure-reducing valve (QTY08, Delisi Group Co., Ltd., China), and a solenoid valve (2V025, Delixi Group Co., Ltd., China). The vibration measurement unit includes a laser Doppler vibrometer (OFV-505, Polytec GmbH, Germany), a data acquisition module (USB-4431, National Instrument, China), and a computer. The vibrometer used was a single-point laser Doppler vibrometer (LDV). The excitation device and the vibrometer are placed 180° apart on opposite sides of the peach, resulting in a high signal-to-noise ratio (Wang et al., 2024). To completely vibrate the on-tree peaches while avoiding damage or dropping, the excitation device provided an approximate transient force at a gas pressure of 300 kPa and an excitation time of 200 ms. The sampling frequency and time of the vibration response were set to 10240 Hz and 5 s, respectively. The vibration measurement was repeated three times for each sample, and the results were averaged.

The reference firmness of each peach was determined by a puncture test using a texture analyser (TA-XT2i, Stable Micro Systems Ltd., United Kingdom) equipped with a cylindrical probe 5 mm in diameter. Each peach was measured at three points that were 120° apart at the equator. The test was conducted at a loading speed of 0.5 mm s⁻¹ and a loading distance of 8 mm. A typical force-displacement curve of a peach is shown in Fig. 2. The initial slope of the force-displacement curve was calculated (Wang et al., 2020). The mean of the three point measurements was recorded as the reference firmness of the peach. The firmness of on-tree peaches at 103–111 DAFB were presented in Table 1. Eventually, 320

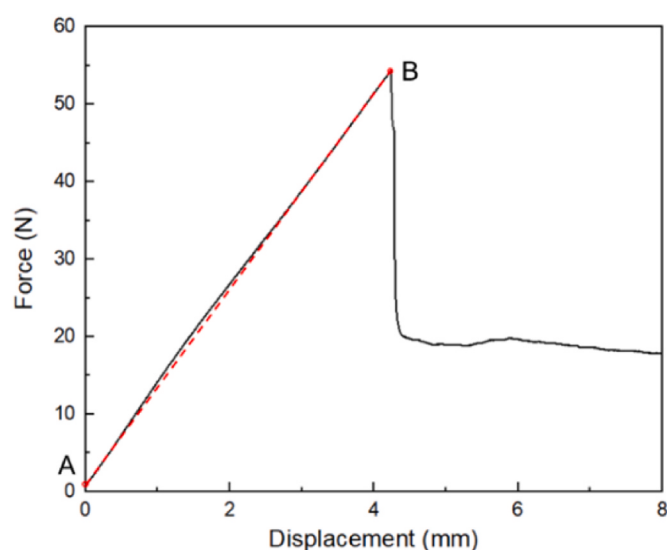


Fig. 2. A typical force-displacement curve of a peach.

Table 1

The firmness measurement results of on-tree peaches at 103–111 days after full bloom.

DAFB	The range of peach firmness (N·mm ⁻¹)	The mean of peach firmness (N·mm ⁻¹)
103	9.74–25.95	14.70
105	6.18–16.79	11.05
107	3.29–16.77	8.09
109	1.55–7.65	3.12
111	1.38–6.21	2.58

experimental vibration response and firmness values were obtained.

The power spectral density (PSD) represents the average power of vibrations as a function of frequency, which offers more information and higher sensitivity than traditional signal processing methods (Xu et al., 2024). The 15th-order autoregressive (AR) method was used to calculate peach PSDs from experimental and simulated vibration responses (Yu et al., 2021). Then the experimental PSDs were divided into training and test sets at a 4:1 ratio. And the 5-fold cross-validation method was employed for model evaluation (Section 2.5).

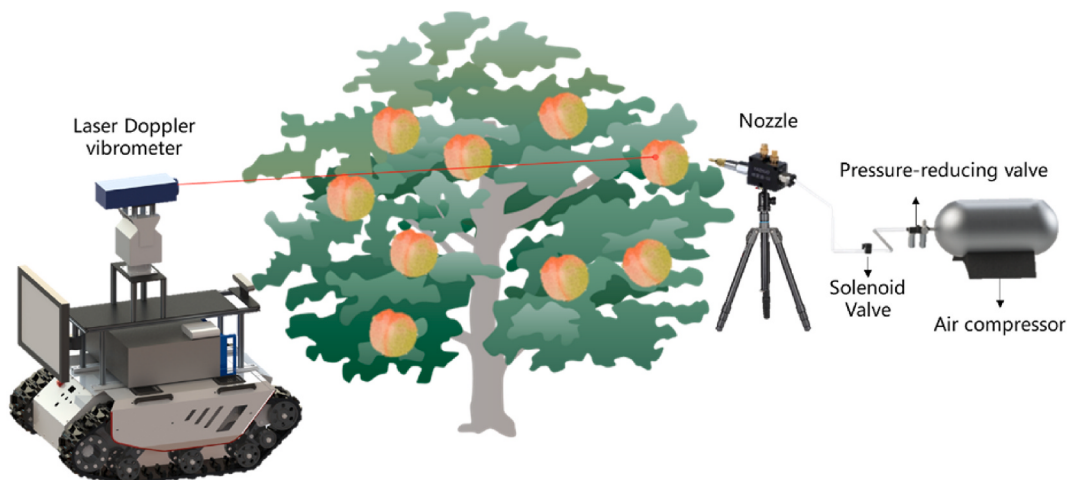


Fig. 1. The device for measuring the acoustic vibration response of on-tree peaches.

2.2.2. D scanning and mechanical property tests

For accurate inversion of peach firmness by acoustic vibration, the dataset was enlarged with the simulated vibration responses generated from high-fidelity FE models of peaches in this study. Since the amount of simulated data was largely determined by the shape, density, elastic modulus, and Poisson's ratio of the FE model, 3D scanning and mechanical property tests were performed to acquire these critical physical and material parameters. A handheld laser scanner (SIMSCAN 30, SCANTECH Co., Ltd., Hangzhou, China) was used to capture 3D point clouds of the external shape as well as the internal structure of the peach. The 3D point clouds of each part were subsequently processed to construct individual NURBS surfaces via Geomagic Studio (Version 2017; Geomagic, Inc., Morrisville, NC). The 3D geometric model of each part was subsequently created via SolidWorks software (version 2020, Dassault Systèmes S.A., Concord, Massachusetts, USA) to establish the high-fidelity FE model of the peach.

The elastic moduli of the flesh, pit and kernel were subsequently measured via compression tests via a texture analyser with a 100 mm diameter compression plate at a 0.1 mm s⁻¹ loading speed and an 8 mm loading distance according to the ASAE standards (S368.4/DEC2000 (R2022)). For the flesh, three cylindrical samples, each with a diameter of 10 mm and a height of 15 mm, were extracted from each peach, and their elastic modulus was calculated using Eq. (1):

$$E = \frac{\sigma}{\epsilon} = \frac{FL}{A\Delta L} \quad (1)$$

where E (MPa) represents the elastic modulus of the flesh and skin, σ (MPa) represents the stress, ϵ represents the strain, F (N) represents the compressive force, L (mm) represents the initial length of the sample, A (mm²) represents the cross-sectional area of the sample, and ΔL (mm) represents the deformation of the sample.

For the pit and kernel, complete pits and kernels were placed on the platform of the texture analyzer to perform compression tests. The curvatures of the top and bottom points were obtained from the 3D solid models via SolidWorks software. The elastic moduli were subsequently calculated according to the ASAE standards (S368.4/DEC2000 (R2022)) using Equation (2):

$$E = \frac{0.338K_U^{3/2}F(1-\mu^2)}{D^{3/2}} \left[K_U \left(\frac{1}{R_U} + \frac{1}{R'_U} \right)^{1/3} + K_L \left(\frac{1}{R_L} + \frac{1}{R'_L} \right)^{1/3} \right]^{\frac{3}{2}} \quad (2)$$

where E (MPa) represents the elastic modulus of the object (e.g. pit and kernel), F (N) represents the compressive force, D (mm) represents the deformation of the object, K_U and K_L are constants determined by the curvatures of the contact points on the upper and lower surfaces, R_U and R'_U are the maximum and minimum radii of curvature (mm) of the contact points on the upper surface, and R_L and R'_L (mm) represent the maximum and minimum radii of curvature of the contact points on the lower surface, the curvature radius of the sample is obtained from the 3D model.

To determine the elastic modulus of the fruit skin, the skin was cut into rectangular strips with a width of 10 mm, length of 20 mm, and thickness of 0.5 mm to perform tensile tests via a universal testing machine (UTM2102, Shenzhen Suns Technology Stock Co., Ltd., Shenzhen, China) (Du et al., 2019). The elastic modulus of the skin was calculated using Equation (1).

In this study, the densities of the fruit flesh, pit, and kernel were obtained by dividing their respective masses by their respective volumes. The mass was measured using an electronic balance (DY15K, Shanghai Jinghai Instrument Co., Ltd., Shanghai, China), whereas the volume was determined using the drainage method. The density of peach skin was considered to be the same as that of peach flesh in this study (Hou et al., 2024).

2.3. High-fidelity FE model and simulation process

The inversion process of on-tree peach firmness is shown in Fig. 3. The first step was to establish high-fidelity FE models of peaches during fruit ripening to generate simulated vibration responses. The simulated data were subsequently used to train the inversion model of peach firmness (Section 2.4). To bridge the gap between the simulated and experimental data, domain adaptation was performed to align the feature distributions between them (Section 2.5).

In this study, high-fidelity FE models of peaches were established on the basis of 3D geometric models of each fruit part and the results of mechanical property tests. A peach is taken as an example to illustrate the modelling process of a high-fidelity FE model. As shown in Fig. 3, after the 3D geometric models were generated (Section 2.2.2), the centroids of each part were first moved to the origin of the coordinates in SolidWorks, and the posture of each part was subsequently adjusted according to the physiological structure of the peach. A combination subtraction operation was subsequently performed to merge the solid models of different parts and ensure that they did not interfere with each other. The individual parts were subsequently assembled into a 3D geometric model of the peach, which was then imported into the FE software ANSYS Workbench (Version 2022 R2, ANSYS, Inc., Canonsburg, PA). The 3D geometric models of the skin, flesh, kernel, pit and the assembled peach were shown in Fig. 4 (a).

In this study, on-tree peaches vibrate under transient excitation. To simulate this scenario, the transient structural module of the software ANSYS Workbench was used. The Young's modulus and density of each part of the peach were set on the basis of the measurement results obtained by mechanical property tests. With reference to previous studies (Nakano et al., 2018), Poisson's ratio was set at 0.35 for the flesh and 0.30 for the skin, pit and kernel. Surface contacts were established between the various parts to form a complete entity. The type and size of the elements were crucial factors influencing the model quality. Tetrahedral elements were chosen for this study since they exhibit good adaptability for irregular shapes, sizes and curvatures and are commonly used for meshing fruit models. For multi-layered peach structures, different element sizes should be chosen on the basis of the shape and size of each part. Considering the quality of the mesh and computational cost, the mesh sizes for the fruit skin, flesh, pit and kernel were set to 2, 5, 3 and 3 mm, respectively. Then the high-fidelity FE model of the peach with 56,205 elements and 101,429 nodes was established (Fig. 4 (b)). For ease of observation and differentiation, the elements of the high-fidelity FE model in different parts are shown in different colours. To simulate real measurement conditions, a fixed constraint was applied at the fruit stem. In this study, the excitation device provided an approximate transient force at a gas pressure of 300 kPa and an excitation time of 200 ms. By comparing the total power of the power spectral density (PSD) signals from simulation and experimental data, the magnitude of the load was determined. Therefore, a transient force of 5 N lasting for 200 ms was applied at a point on the equator in the X-axis direction (the laser direction of the LDV). The opposite point on the equator was chosen as the measurement point of the vibration response, and the vibration velocity along the X-axis at this point was recorded. The simulation duration was set to 1 s with 10240 substeps.

By following the above steps, ten high-fidelity FE models of peaches of different sizes and shapes were established during fruit ripening. To generate the simulated vibration responses from the FE models of the peaches, the material parameters of these models were tuned according to the measurement results of different parts of the peaches via the mechanical property tests in Table 2. The elastic moduli of the flesh were regarded as the firmness of the simulated peach. Since the experimental elastic modulus measured by the texture analyzer has a precision of 0.01 MPa, the step size of the elastic modulus variation was set to 0.01 MPa during the simulation to ensure the similarity between the simulated and experimental data. Consequently, a total of 1000 simulated vibration response of the peaches were obtained by varying the elastic moduli

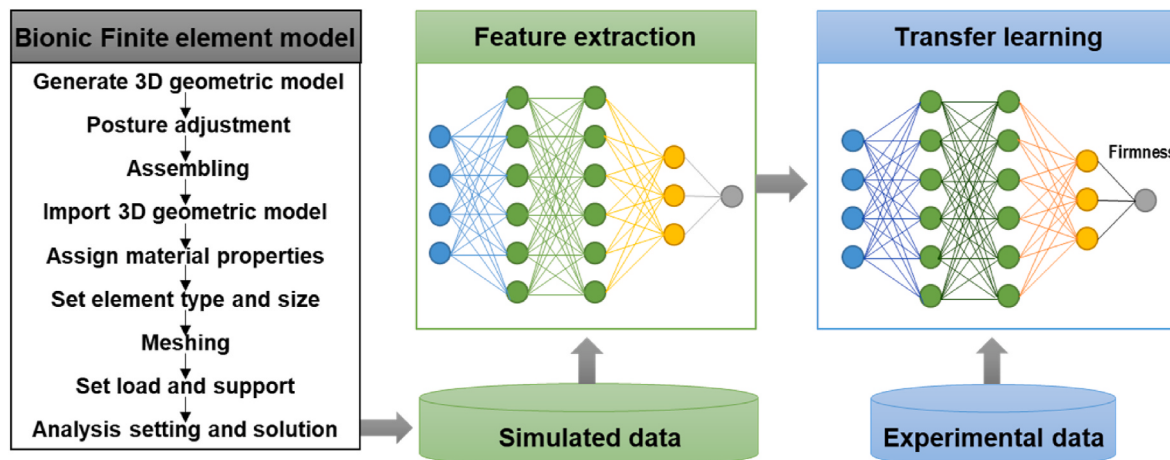


Fig. 3. The inversion process of on-tree peach firmness.

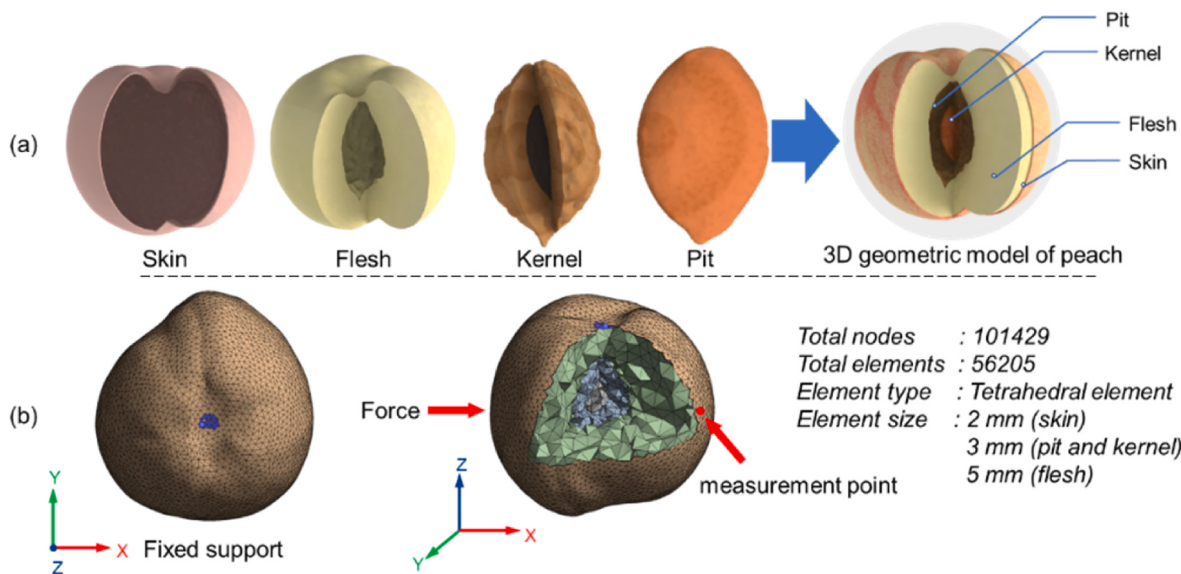


Fig. 4. The established 3D geometric model (a) and high-fidelity finite element model (b) of a typical peach.

Table 2

The measurement results of different parts of 'Dongxi Xiaoxian' peaches by mechanical property test.

Material parameters	Peach parts			
	Skin	Flesh	Pit	Kernel
Young's modulus (MPa)	2.74–6.67	0.23–3.81	248.43–347.79	8.64–13.34
Density (kg·m ⁻³)	980	980	1285	1170

of the flesh. The PSDs of simulated data were calculated by using 15th-order autoregressive method. Subsequently, the simulated PSDs were also divided into training and test sets at a ratio of 4:1.

2.4. Deep transfer learning for peach firmness inversion

2.4.1. D-Inception-SE network

To extract features from the vibration responses for characterising peach firmness, a 1D-Inception-SE network was constructed. As shown in Fig. 5 (a), its structure comprises two convolutional layers: a 1D-Inception module, a squeeze-and-excitation (1D-SE) module, a dropout layer, and two fully connected (FC) layers.

Convolutional layers were used for vibration feature extraction. Since the vibration responses are one-dimensional data, a one-dimensional convolutional neural network (1D-CNN) was adopted as the fundamental architecture of the network. The 1D-CNN architecture consists of input layers, convolutional layers, pooling layers, fully connected layers, and output layers (Junior et al., 2022). It has multiple convolutional layers and fewer parameters, which enable strong local feature extraction and significantly reduce computational complexity (Kiranyaz et al., 2021). In addition, the Inception module (Szegedy et al., 2015) was introduced to prevent overfitting potentially caused by incorporating additional convolutional layers. It embodies a multi-branch structure, with each branch having convolutional kernels of different sizes, enabling the extraction of multiscale features from the vibration responses (Shi et al., 2017). In this study, the kernel sizes of the Inception module were modified to adapt to one-dimensional signals. Fig. 5 (b) shows the structure of the 1D-Inception module.

To allocate more attention to important channel information, the squeeze-and-excitation (SE) module was adopted (Chen et al., 2022). The SE module is a representative channel attention mechanism designed for processing two-dimensional data such as images; it learns the importance of different feature channels and models the interdependencies among them (Hu et al., 2018). Since the vibration

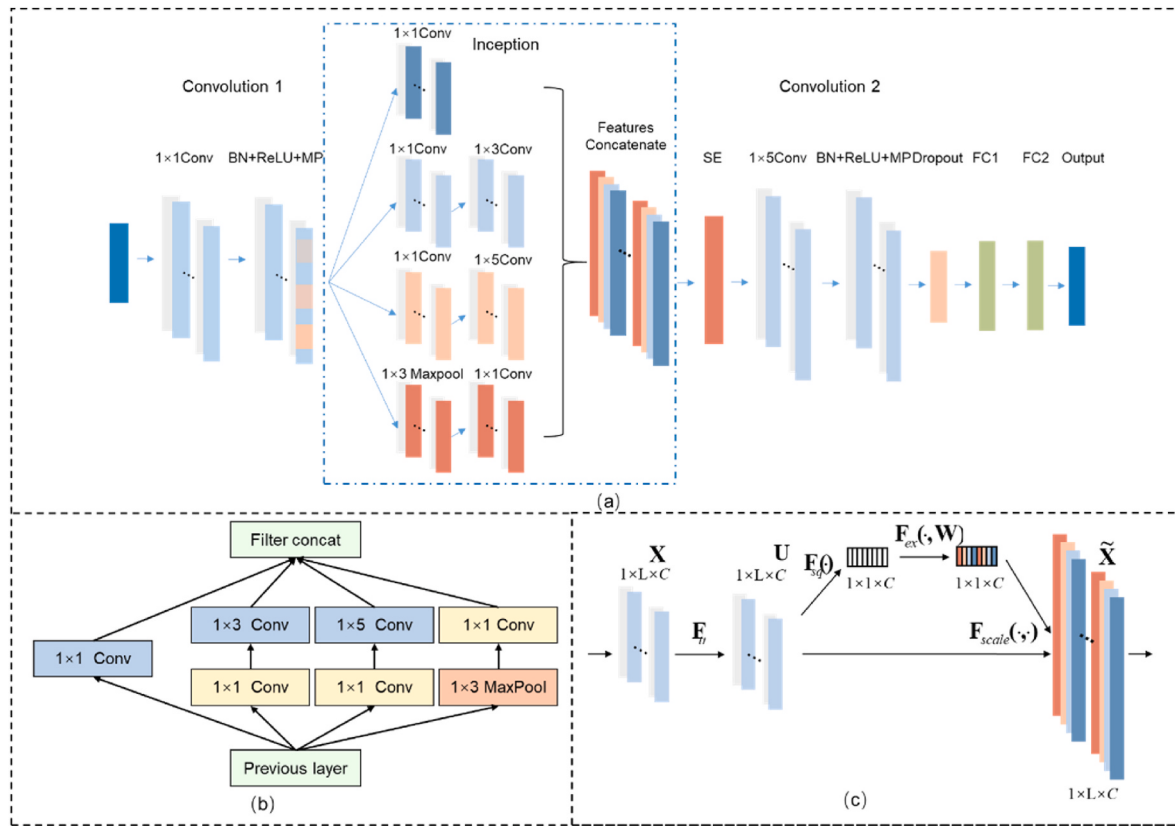


Fig. 5. Architecture of the proposed 1D-Inception-SE network (a), the 1D-Inception module (b) and the 1D-SE module (c).

response is a one-dimensional signal with a length of L , the SE module was modified to accommodate one-dimensional data processing, and its structure is illustrated in Fig. 5 (c). The input data consist of C vibration signals with dimensions of $1 \times L \times C$. The 1D-SE module involves two operations: squeeze and excitation. First, the squeeze operation compresses the features from $1 \times L \times C$ to $1 \times 1 \times C$ through global average pooling to obtain a real-valued sequence $Z \in R^C$. The n -th element of Z can be defined as follows:

$$Z_n = \frac{1}{1 \times L} \sum_{i=1}^L u_c(i) \quad (4)$$

where L represents the length of the vibration signal and $u_c(i)$ represents the value of the i -th feature of the c -th vibration signal.

In the excitation operation, two fully connected layers are employed to apply the sigmoid function for feature activation, thereby generating attention weights (W_1 and W_2) for each channel. Suppose that $W_1 \in R^{N_r \times N}$ and $W_2 \in R^{N \times N_r}$ are two fully connected layers. The excitation operation can be described by the following equation:

$$F_{ex}(z, W) = \sigma(g(z, W)) = \sigma(W_2 \delta(W_1 z)) \quad (5)$$

where σ is the sigmoid function, δ is the ReLU activation function, N is the input channel number, and r is a reduction ratio used to constrain the model complexity.

Finally, the computed weights were multiplied by the channel features to enhance crucial features and attenuate less relevant features. Moreover, batch normalization layers, ReLU activation layers, and max pooling layers were added to accelerate model training and enhance the model's nonlinearity. A dropout layer was used to reduce redundant features and enhance the robustness of the model.

2.4.2. Domain adversarial neural network

This study aims to enhance the performance of the firmness inversion

model for on-tree peaches by expanding the sample capacity using simulated data obtained from FE peach models. Since there is an inevitable gap between simulated data (source domain) and experimental data (target domain), employing models trained with simulated data for processing experimental data may introduce errors (Su et al., 2023). Domain adaptation, as an important subfield of transfer learning, aims to address such domain shifts. In this study, a domain adversarial neural network (DANN) is employed to align the feature distributions between the source domain ($\mathcal{D}_{source} = \{x_s, y_s\}_{s=1}^{N_s}$) and target domain ($\mathcal{D}_{target} = \{x_t, y_t\}_{t=1}^{N_t}$). The network consists of a feature extractor $G_f(\cdot, \theta_f)$, predictor $G_p(\cdot, \theta_p)$ and domain classifier $G_d(\cdot, \theta_d)$, as illustrated in Fig. 6. The feature extractor maps the data into a feature space, the domain classifier distinguishes between the target and source domains via the gradient reversal layer (GRL), and the predictor is used to predict firmness. While the predictor is trained to obtain the best firmness prediction accuracy, the domain classifier is trained to obtain the maximum domain classification loss, so the feature extractor can simultaneously extract the domain-invariant features and obtain the optimal firmness prediction accuracy.

The mean squared error (MSE) and binary cross-entropy are chosen as the loss functions for the predictor and domain classifier, respectively. The loss function is given by the following equations:

$$\mathcal{L} = \mathcal{L}_p - \lambda \mathcal{L}_d \quad (6)$$

$$\mathcal{L}_p = \frac{\sum_{i=1}^{N_s} (y_i - \hat{y}_i)^2}{N_s} \quad (7)$$

$$\mathcal{L}_d = \frac{1}{N_s + N_t} \sum_{i=1}^{N_s+N_t} y_i \log \hat{y}_i + (1 - y_i) \log(1 - \hat{y}_i) \quad (8)$$

where \mathcal{L} is the total loss function, \mathcal{L}_p represents the predictor loss of

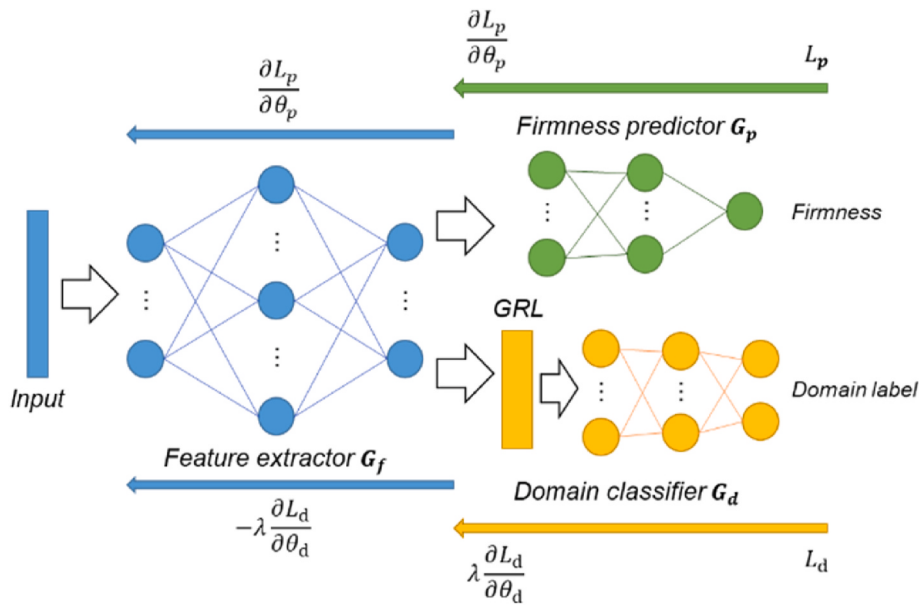


Fig. 6. Architecture of DANN.

fruit firmness, \mathcal{L}_d represents the domain classifier loss, λ is a weight parameter that balances the relative importance of \mathcal{L}_p and \mathcal{L}_d , N_s denotes the number of samples in the source domain, y_i represents the true label of the i -th sample, \hat{y}_i represents the predicted label of the i -th sample, and N_T denotes the number of samples in the target domain. The pseudocode of DANN was presented in Table 3.

2.5. Model training and evaluation

The 5-fold cross-validation method (Xu et al., 2025) was adopted to evaluate firmness inversion models for on-tree peaches. The dataset was randomly divided into 5 folds. Over 5 iterations, each fold served once as the test set while the remaining 4 folds constituted the training set. The root mean square error (RMSE) and coefficient of determination (R^2) for

Table 3
Pseudocode implementation of the Domain Adversarial Neural Network.

Algorithm 1 Domain Adversarial Neural Network (DANN)

```

Input: Source data  $X_s$ ,  $Y_s$ , Target data  $X_t$ ,  $Y_t$ , learning rate  $\eta$ , weight parameter  $\lambda$  for epoch = 1 to N do
Sample batch:  $(x_s, y_s) \sim X_s, Y_s$ ,  $x_t \sim X_t$ 
Feature extraction:  $f_s = G_f(x_s)$ ,  $f_t = G_f(x_t)$ 
Prediction loss:  $L_p = \text{Mean squared error}(G_p(f_s), y_s)$ 
Domain discriminator input:  $f = \text{concat}(f_s, f_t)$ 
Domain labels:  $d = (0, 1)$ , 0 for source, 1 for target
Domain loss:  $L_d = \text{Binary cross-entropy}(G_d(f), d)$ 
Gradient Reversal Layer (GRL):  $\nabla L_d \leftarrow \lambda \nabla \mathcal{L}_d$ 
Total loss:  $\mathcal{L} = \mathcal{L}_p + \mathcal{L}_d$ 
Update parameters:  $\theta_{f,y} \leftarrow \theta_{f,y} - \eta \nabla \mathcal{L}$ , Update feature extractor and classifier
Update parameters:  $\theta_d \leftarrow \theta_d - \eta \nabla L_d$ , Update domain discriminator
end for
Output: Feature extractor  $G_f$ , Domain Classifier  $G_d$ 
```

Note: x_s is the input feature from the source domain, y_s is the corresponding label of x_s , N_s denotes the number of samples in the source domain, x_t is the input feature from the target domain, and y_t is the corresponding label of x_t , N_T denotes the number of samples in the target domain. G_f is the feature extractor, G_d the domain classifier, f_s means extracting features from x_s using G_f , f_t means extracting features from x_t using G_f , f is the domain discriminator input, \mathcal{L} is the total loss function, \mathcal{L}_p represents the predictor loss of fruit firmness, \mathcal{L}_d represents the domain classifier loss, $\nabla \mathcal{L}$ is the gradient of the total loss and ∇L_d is the gradient of the domain loss.

Table 4
Hyperparameters used for training firmness inversion models for on-tree peaches.

Hyperparameter	Firmness inversion models for on-tree peaches
Momentum	0.9
Batch size	64
Dropout rate	0.3
Regularization coefficient	0.0001
Learning rate	0.001
Maximum epoch	100

each test fold were calculated using equations (9) and (10). The average scores of RMSE and R^2 across all folds were recorded as evaluation metrics to quantitatively assess the model's performance in firmness prediction.

$$\text{RMSE} = \sqrt{\frac{\sum_{i=1}^n (y_i - \hat{y}_i)^2}{n}} \quad (9)$$

$$R^2 = 1 - \frac{\sum_{i=1}^n (y_i - \hat{y}_i)^2}{\sum_{i=1}^n (y_i - \bar{y})^2} \quad (10)$$

The parameters used for model training are shown in Table 4. The model was implemented on a Windows 10 operating system equipped with an Intel Core i5-12400 processor and an NVIDIA GeForce RTX 3060Ti 16 GB GPU. The experimental code was implemented using the PyTorch deep learning library in Python.

3. Results and discussion

3.1. High-fidelity FE model and simulated vibration responses

Fig. 7 shows the measured and simulated PSD spectra of on-tree peaches with different firmness values. The measured PSD spectra exhibited clear peaks, and the peaks tended to shift to lower frequencies with increasing firmness, as determined by the puncture test. A similar trend was presented in the simulated PSD spectra, which were generated from the high-fidelity FE peach model with different elastic moduli to simulate firmness changes. Moreover, some differences were also

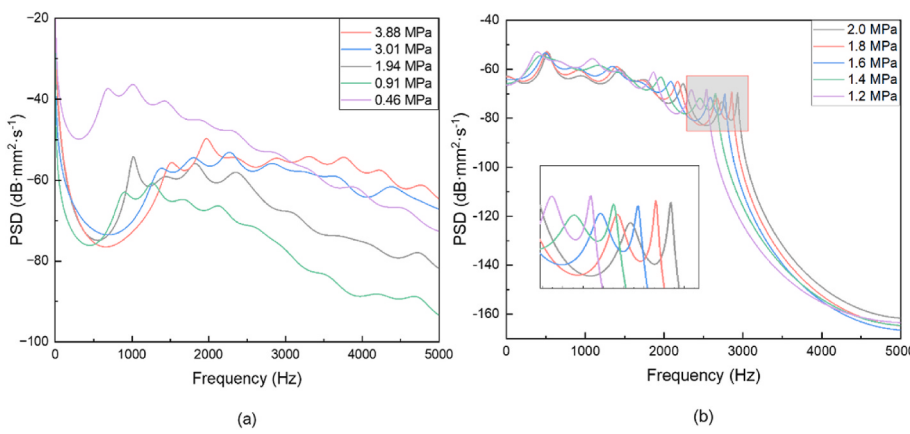


Fig. 7. Experimental (a) and simulated (b) PSD spectra of on-tree peaches with different firmness.

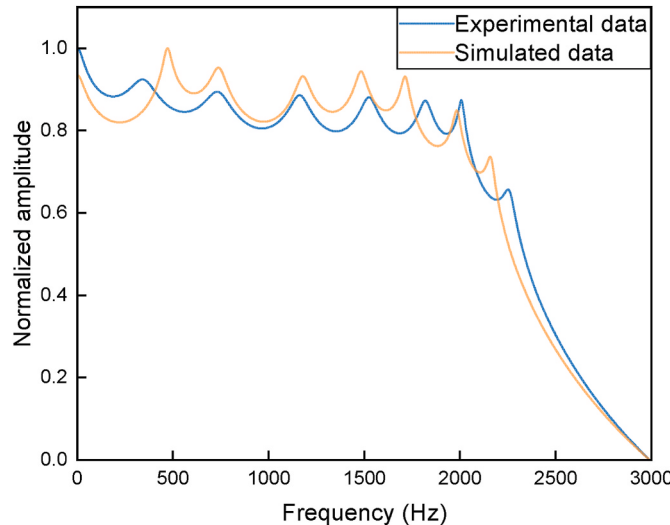


Fig. 8. Comparison of normalized experimental and simulated PSD spectra of the same peach.

observed. The difference between the experimental PSD spectra of peaches with different firmness values was significant, but that of the simulated data was not as obvious. The main reason might be related to the samples. The actual peaches varied greatly in size and shape, whereas only 10 high-fidelity FE models of peaches were established in this study. This might have led to the similarity between the simulated data. The other reason might be the excitation force. The excitation force was consistent in the simulation process. However, ensuring that the distance between the excitation device and the peach was equal during the measurement in the orchard was difficult, which resulted in a slight difference in excitation force. Moreover, the outdoor orchard environment was more complicated than the simulation environment was. Owing to the interference of ambient wind, the measured PSD spectra were inevitably polluted by noise, resulting in less pronounced peaks than those in the simulated data.

According to the comparison results in Fig. 7, the amplitude of the PSD spectrum was normalized to reduce the influence of the exciting force, and a low-pass filter was used to remove the frequency components above 2000 Hz from the normalized PSD spectrum (Diezma-Iglesias et al., 2006; Simón-Portillo et al., 2023; Wang et al., 2004). Fig. 8 shows the experimental data and the simulated data for the same peach. The average cosine similarity between the simulated and experimental curves of the 10 peaches was 0.994, which showed that they had high similarity. The results indicated that the simulated data output by the high-fidelity FE models of the peaches were reliable.

3.2. Performance evaluation and comparisons

There was a gap between the simulated data (the source domain) and the experimental data (the target domain). The model established with the simulated data may produce inaccurate predictions for the experimental data. To alleviate this situation, the DANN was used to align the feature distributions between the source domain and the target domain. The distributions of the extracted features before and after domain adaptation were visualized by the t-distributed stochastic neighbor embedding (t-SNE) algorithm (Maaten & Hinton, 2008). The results are illustrated in Fig. 9. Before domain adaptation, the feature distribution of the target domain was larger and more uniform. However, the features of the source domain were concentrated in a few regions, possibly due to the small number of models. This result indicated that the distributions of the extracted features of the simulated data were obviously different from those of the experimental data. Hence, using the model trained on simulated data to process experimental data would extract invalid features, resulting in reduced firmness prediction accuracy. The features of the source and target domains after domain adaptation are shown in Fig. 9 (b). After domain adaptation, the feature distribution ranges of the two domains aligned closely, and a more uniform distribution was exhibited. The results of feature visualization indicated that the DANN effectively reduced the difference between the experimental data and the simulated data.

To validate the effectiveness of the 1D-Inception-SE network and transfer learning and explain the effectiveness of each component of the 1D-Inception-SE network, ablation experiments were designed on the basis of multiscale convolution (1D-Inception), an attention mechanism (1D-SE), and transfer learning (DANN). As shown in Table 5, the R^2 and RMSE of the test set of 1D-Inception were 0.69 and 3.09 N mm^{-1} , respectively; the R^2 and RMSE of the test set of 1D-SE were 0.75 and 2.75 N mm^{-1} , respectively; and the R^2 and RMSE of the test set of 1D-Inception-SE were 0.79 and 2.51 N mm^{-1} , respectively. Compared to the 1D-Inception (CNN_m) constructed by Wang et al. (2022), the 1D-Inception-SE model achieved a 14.49 % increase in R^2 and a 18.77 % reduction in RMSE on the same dataset in this study. Relative to the 1D-SE model, the 1D-Inception-SE model improved R^2 by 5.33 % and reduced RMSE by 8.73 %. The results indicated that the SE module exerted a more pronounced influence on model performance, but the combination of both modules enabled the extraction of more effective information from the multiscale features, thereby further enhancing model performance. With the introduction of transfer learning, the 1D-Inception-SE-DANN model achieved a 5.06 % increase in R^2 and a 9.16 % reduction in RMSE on the test set compared with the 1D-Inception-SE model. The results showed that the proposed deep transfer learning method could effectively improve the inversion accuracy of peach firmness.

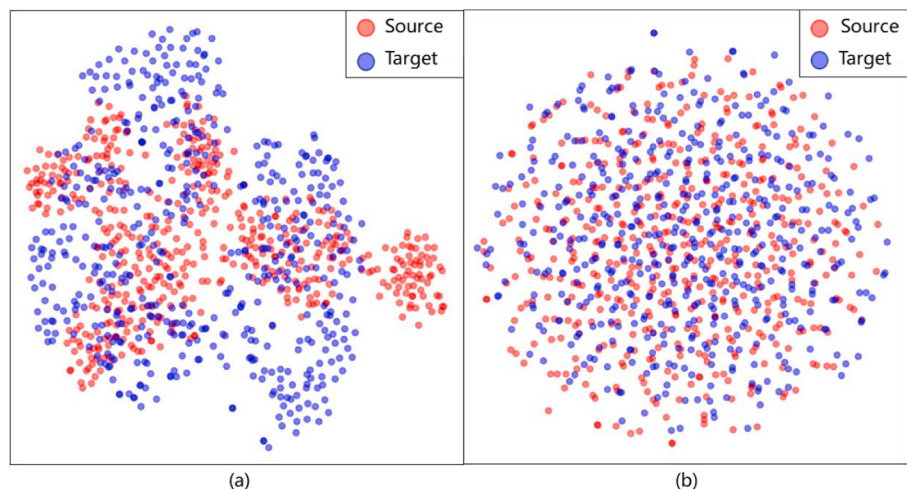


Fig. 9. t-SNE visualization of original features (a) and extracted features (b) by DANN. The red colour represents the features extracted from the simulated data (Source), whereas the blue colour represents the features extracted from the experimental data (Target). (For interpretation of the references to colour in this figure legend, the reader is referred to the Web version of this article.)

Table 5
Ablation experiment results of firmness inversion models for on-tree peaches.

Models	Inputs	R ²	RMSE (N·mm ⁻¹)
1D-Inception	320 experimental data	0.69	3.09
1D-SE	320 experimental data	0.75	2.75
1D-Inception-SE	320 experimental data	0.79	2.51
1D-Inception-DANN	1000 simulated and 320 experimental data	0.72	2.91
1D-SE-DANN	1000 simulated and 320 experimental data	0.79	2.63
1D-Inception-SE-DANN	1000 simulated and 320 experimental data	0.83	2.28

Note: R² is the coefficient of determination; RMSE means the root mean square error.

To evaluate the performance of the proposed method under conditions with limited experimental samples, deep transfer learning experiments were conducted using 25 % (80), 50 % (160), 75 % (240), and 100 % (320) of the available data. The results are presented in **Table 6**. As the number of experimental samples increased, the performance of both the deep learning model (1D-Inception-SE) and the deep transfer learning model (1D-Inception-SE-DANN) continuously improved. When the same number of experimental samples were used, the performance of the 1D-Inception-SE-DANN models was superior to that of the 1D-Inception-SE models, notably achieving a 20.34 % increase in R² with a sample size of 80 peaches. Compared to the 1D-Inception-SE model trained with 160 experimental samples, the 1D-Inception-SE-DANN trained with simulated data and 80 experimental samples achieved nearly equivalent performance. When trained with simulated data and 160 experimental samples, the 1D-Inception-SE-DANN model outperformed the 1D-Inception-SE model trained with 320 experimental samples, even though the latter used twice as many samples. The results demonstrated that the proposed method can effectively reduce the number of samples required while achieving excellent results. When the sample size reached 240, the 1D-Inception-SE-DANN model achieved the highest R² of 0.83. As the sample size continued to increase, the R² no longer improved, but the RMSE continued to decrease. The results indicate that the proposed method can effectively increase inversion accuracy and reduce inversion error for on-tree peach firmness, even with a small sample size.

Table 6
The performance of firmness inversion models for on-tree peaches based on deep transfer learning with varying inputs and sample sizes.

Models	Inputs	R ²	RMSE (N·mm ⁻¹)
1D-Inception-SE	80 Experimental samples	0.59	3.64
1D-Inception-SE	160 Experimental samples	0.72	3.13
1D-Inception-SE	240 Experimental samples	0.76	2.81
1D-Inception-SE	320 Experimental samples	0.79	2.51
1D-Inception-SE-DANN	1000 simulated and 80 experimental samples	0.71	3.15
1D-Inception-SE-DANN	1000 simulated and 160 experimental samples	0.81	2.51
1D-Inception-SE-DANN	1000 simulated and 240 Experimental samples	0.83	2.32
1D-Inception-SE-DANN	1000 simulated and 320 Experimental samples	0.83	2.28

Note: R² is the coefficient of determination; RMSE means the root mean square error.

3.3. Limitations and perspective

This study proposes an innovative method for peach fruit firmness inversion based on high-fidelity FE models and deep transfer learning, and has achieved satisfactory results under conditions of limited samples. However, there are still some limitations to this research. Firstly, the study was only tested on a single variety of peaches and has not yet explored the applicability of this method to other varieties. Secondly, the constraints on the peach stem were simplified during the computational simulation, which does not fully capture the complex physical characteristics of peaches as they grow in natural environments. Additionally, while the deep transfer learning method based on adversarial neural networks effectively reduced the feature distribution differences between the simulated and experimental datasets, these differences were not completely eliminated. Lastly, although this study achieved non-contact measurement of the fruit, the measurement process still needs manual alignment, which limits the improvement of detection efficiency.

The results of this study can accurately invert the firmness of peaches on the tree, which is helpful for monitoring their ripeness and determining the optimal harvest time. Future research will first verify the feasibility of this method for firmness inversion of different peach

varieties. On this basis, the efficiency and accuracy of this method will be further improved through the following steps: a) developing an automated vibration measurement system for on-tree fruits to improve detection efficiency; b) further optimizing the stem constraint settings during the computational simulation to more closely match the actual growth conditions of peaches; c) making improvements to the deep transfer learning method to further reduce domain discrepancies.

Moreover, the proposed method of this study is not only applicable to peaches, but also can be extended to other drupes with similar internal structure to peaches, such as apricots and plums. Utilizing the LDV-based vibration measurement method and the mechanical property testing method (Section 2.2), the experimental vibration data and elastic modulus of the specific drupe can be obtained. By following the FE model construction method (Section 3), high-fidelity FE models and simulation data for specific drupe can be obtained. Adopting the proposed deep transfer learning method (Section 2.4), the firmness inversion models for the specific drupe can be established.

4. Conclusions

An acoustic vibration method based on high-fidelity FE modelling and deep transfer learning for the inversion of the on-tree peach firmness was proposed and tested. Ten high-fidelity FE models of peaches comprising the skin, flesh, pit and kernel were established to generate 1000 simulated vibration responses of on-tree peaches during fruit ripening. The average cosine similarity between the PSDs of the simulation data and experimental data was 0.994, which indicated that the simulated data output by the high-fidelity FE model had high similarity with the experimental data. The 1D-Inception-SE model achieved good performance in extracting vibration features from the PSDs for characterising peach firmness and assessing the firmness of on-tree peaches, compared to the reported 1D-Inception (CNN_m) model, the R² of the 1D-Inception-SE model increased by 14.49 %, and the RMSE decreased by 18.77 %. Compared with the inversion model trained with only experimental data, the deep transfer learning method improved the performance of the inversion model for on-tree peach firmness, with a 5.06 % increase in R² and a 9.16 % reduction in the RMSE of the test set. Moreover, the performance of the deep transfer learning model trained with simulated data and 160 experimental samples surpassed that of the 1D-Inception-SE model trained with 320 experimental samples, even though the latter used twice as many samples. When the sample size reached 240, the 1D-Inception-SE-DANN model achieved the highest R² of 0.83. As the sample size continued to increase, the R² no longer improved, but the RMSE continued to decrease. The results demonstrated that the proposed deep transfer learning method could achieve accurate inversion for on-tree peach firmness during fruit ripening with a limited number of samples. In the future, a visual guiding system will be constructed to automatically perform vibration measurements for on-tree peaches to improve efficiency.

CRediT authorship contribution statement

Jiaqi Xiong: Writing – review & editing, Writing – original draft, Software, Investigation, Data curation. **Yilei Hu:** Writing – review & editing, Software. **Xianbin Gu:** Writing – review & editing, Methodology. **Ce Yang:** Writing – review & editing. **Di Cui:** Writing – review & editing, Resources, Project administration, Methodology, Funding acquisition.

Declaration of competing interest

The authors declare that they have no known competing financial interests or personal relationships that could have appeared to influence the work reported in this paper.

Acknowledgments

The authors gratefully acknowledge the support of this program by the National Natural Science Foundation of China (Grant No. 31571764), China.

References

- Abbaszadeh, R., Rajabipour, A., Sadrnia, H., Mahjoob, M. J., Delshad, M., & Ahmadi, H. (2014). Application of modal analysis to the watermelon through finite element modeling for use in ripeness assessment. *Journal of Food Engineering*, 127, 80–84. <https://doi.org/10.1016/j.jfooodeng.2013.11.020>
- Castiglioni, I., Rundo, L., Codari, M., Di Leo, G., Salvatore, C., Interlenghi, M., Gallivanone, F., Cozzi, A., D'Amico, N. C., & Sardanelli, F. (2021). AI applications to medical images: From machine learning to deep learning. *Physica Medica*, 83, 9–24. <https://doi.org/10.1016/j.ejmp.2021.02.006>
- Chen, X., Gao, W., Hong, C., & Tu, Y. (2022). A novel series arc fault detection method for photovoltaic system based on multi-input neural network. *International Journal of Electrical Power & Energy Systems*, 140, Article 108018. <https://doi.org/10.1016/j.ijepes.2022.108018>
- Diezma-Iglesias, B., Valero, C., García-Ramos, F. J., & Ruiz-Altsent, M. (2006). Monitoring of firmness evolution of peaches during storage by combining acoustic and impact methods. *Journal of Food Engineering*, 77(4), 926–935. <https://doi.org/10.1016/j.jfooodeng.2005.08.021>
- Ding, C., Wang, D., Feng, Z., & Cui, D. (2022). Detection of apple firmness with a novel loudspeaker-based excitation device. *International Journal of Agricultural and Biological Engineering*, 15(1), 260–266. <https://doi.org/10.25165/j.ijabe.20221501.7028>
- Du, D., Wang, B., Wang, J., Yao, F., & Hong, X. (2019). Prediction of bruise susceptibility of harvested kiwifruit (*Actinidia chinensis*) using finite element method. *Postharvest Biology and Technology*, 152, 36–44. <https://doi.org/10.1016/j.postharvbio.2019.02.013>
- Ganin, Y., Ustinova, E., Ajakan, H., Germain, P., Larochelle, H., Laviolette, F., Marchand, M., & Lempitsky, V. (2017). Domain-adversarial training of neural networks. In G. Csurka (Ed.), *Domain adaptation in computer vision applications* (pp. 189–209). Springer International Publishing. https://doi.org/10.1007/978-3-319-58347-1_10
- Gonçalves, R. G., Couto, J., & Almeida, D. P. F. (2016). On-tree maturity control of peach cultivars: Comparison between destructive and nondestructive harvest indices. *Scientia Horticulturae*, 209, 293–299. <https://doi.org/10.1016/j.scienta.2016.06.040>
- Hou, J., Park, B., Li, C., & Wang, X. (2024). A multiscale computation study on bruise susceptibility of blueberries from mechanical impact. *Postharvest Biology and Technology*, 208, Article 112660. <https://doi.org/10.1016/j.postharvbio.2023.112660>
- Hu, J., Shen, L., & Sun, G. (2018). Squeeze-and-Excitation networks. *2018 IEEE/CVF conference on computer vision and pattern recognition* (pp. 7132–7141). <https://doi.org/10.1109/CVPR.2018.00745>
- Junior, R. F. R., Areias, I. A. D. S., Campos, M. M., Teixeira, C. E., Da Silva, L. E. B., & Gomes, G. F. (2022). Fault detection and diagnosis in electric motors using 1d convolutional neural networks with multi-channel vibration signals. *Measurement*, 190, Article 110759. <https://doi.org/10.1016/j.measurement.2022.110759>
- Kiranyaz, S., Avci, O., Abdeljaber, O., Ince, T., Gabboj, M., & Inman, D. J. (2021). 1D convolutional neural networks and applications: A survey. *Mechanical Systems and Signal Processing*, 151, Article 107398. <https://doi.org/10.1016/j.msssp.2020.107398>
- Kondo, N., Nishizu, T., Hayashi, T., Ogawa, Y., Shimizu, H., & Goto, K. (2014). *Physical and biological properties of agricultural products*. Kyoto, Japan: Kyoto University Press. ISBN: 9784876983896.
- Landahl, S., & Terry, L. A. (2020). Non-destructive discrimination of avocado fruit ripeness using laser Doppler vibrometry. *Biosystems Engineering*, 194, 251–260. <https://doi.org/10.1016/j.biosystemseng.2020.04.001>
- Lin, J., Hu, Q., Xia, J., Zhao, L., Du, X., Li, S., Chen, Y., & Wang, X. (2023). Non-destructive fruit firmness evaluation using a soft gripper and vision-based tactile sensing. *Computers and Electronics in Agriculture*, 214, Article 108256. <https://doi.org/10.1016/j.compag.2023.108256>
- Lou, Y., Kumar, A., & Xiang, J. (2023). Machinery fault diagnostic method based on numerical simulation driving partial transfer learning. *Science China Technological Sciences*, 66(12), 3462–3474. <https://doi.org/10.1007/s11431-023-2496-6>
- Lu, J., Behbood, V., Hao, P., Zuo, H., Xue, S., & Zhang, G. (2015). Transfer learning using computational intelligence: A survey. *Knowledge-Based Systems*, 80, 14–23. <https://doi.org/10.1016/j.knosys.2015.01.010>
- Luo, X., Chen, L., Liang, T., & Huang, T. (2024). Structural damage identification for bridges based on transfer learning and 1-D convolutional neural network. *Journal of Railway Science and Engineering*, 21(9), 1–12. <https://doi.org/10.19713/j.cnki.43-1423/u.T20231981>
- Ma, C., Ying, Y., & Xie, L. (2024). Visuo-tactile sensor development and its application for non-destructive measurement of peach firmness. *Computers and Electronics in Agriculture*, 218, Article 108709. <https://doi.org/10.1016/j.compag.2024.108709>
- Maaten, L. van der, & Hinton, G. (2008). Visualizing data using t-SNE. *Journal of Machine Learning Research*, 9(86), 2579–2605.
- Melo Junior, W. W. A. D., Santos, F. L., Scinocca, F., Rosa, P. A. D., & Magalhães, R. R. (2024). Dynamic behavior of coffee branches: An analysis using the finite element method. *Brazilian Archives of Biology and Technology*, 67, Article e24220331. <https://doi.org/10.1590/1678-4324-2024220331>

- Nakano, R., Akimoto, H., Fukuda, F., Kawai, T., Ushijima, K., Fukamatsu, Y., Kubo, Y., Fujii, Y., Hirano, K., Morinaga, K., & Sakurai, N. (2018). Nondestructive detection of split pit in peaches using an acoustic vibration method. *The Horticulture Journal*, 87(2), 281–287. <https://doi.org/10.2503/hortj.OKD-094>
- Nouri, S. F., & Abdanan Mehdizadeh, S. (2024). Design, construction and evaluation of a device for non-destructive measurement of firmness in fruits using vibration analysis (case study: Kiwifruit). *Scientia Horticulturae*, 328, Article 112965. <https://doi.org/10.1016/j.scienta.2024.112965>
- Pereira, J. S., Magalhães, R. R., & Santos, F. L. (2023). Modeling of coffee fruit: An approach to simulate the effects of compression. *AgriEngineering*, 5(4), 2303–2313. <https://doi.org/10.3390/agriengineering5040141>
- Rashvand, M., Altieri, G., Genovese, F., Li, Z., & Di Renzo, G. C. (2022). Numerical simulation as a tool for predicting mechanical damage in fresh fruit. *Postharvest Biology and Technology*, 187, Article 111875. <https://doi.org/10.1016/j.jpostharvbio.2022.111875>
- Shi, W., Jiang, F., & Zhao, D. (2017). Single image super-resolution with dilated convolution based multi-scale information learning inception module. *2017 IEEE international conference on image processing (ICIP)* (pp. 977–981). <https://doi.org/10.1109/ICIP.2017.8296427>
- Simón-Portillo, F. J., Abellán-López, D., Fabra-Rodríguez, M., Peral-Orts, R., & Sánchez-Lozano, M. (2023). Detection of hollow heart disorder in watermelons using vibrational test and machine learning. *Journal of Agriculture and Food Research*, 14, Article 100779. <https://doi.org/10.1016/j.jafr.2023.100779>
- Su, S., Li, W., Mou, J., Garg, A., Gao, L., & Liu, J. (2023). A hybrid battery equivalent circuit model, deep learning, and transfer learning for battery state monitoring. *IEEE Transactions on Transportation Electrification*, 9(1), 1113–1127. <https://doi.org/10.1109/TTE.2022.3204843>
- Szegedy, C., Liu, W., Jia, Y., Sermanet, P., Reed, S., Anguelov, D., Erhan, D., Vanhoucke, V., & Rabinovich, A. (2015). Going deeper with convolutions. *2015 IEEE conference on computer vision and pattern recognition (CVPR)* (pp. 1–9). <https://doi.org/10.1109/CVPR.2015.7298594>
- Wang, D., Ding, C., Feng, Z., & Cui, D. (2020). A low-cost handheld apparatus for inspection of peach firmness by sensing fruit resistance. *Computers and Electronics in Agriculture*, 174, Article 105463. <https://doi.org/10.1016/j.compag.2020.105463>
- Wang, D., Feng, Z., Ji, S., & Cui, D. (2022). Simultaneous prediction of peach firmness and weight using vibration spectra combined with one-dimensional convolutional neural network. *Computers and Electronics in Agriculture*, 201, Article 107341. <https://doi.org/10.1016/j.compag.2022.107341>
- Wang, D., Hu, Y., Xiong, J., Ying, Y., Yang, C., & Cui, D. (2024). Laser Doppler vibrometer enables in-situ monitoring of peach firmness. *Biosystems Engineering*, 247, 191–201. <https://doi.org/10.1016/j.biosystemseng.2024.09.013>
- Wang, J., Teng, B., & Yu, Y. (2004). Pear dynamic characteristics and firmness detection. *European Food Research and Technology*, 218(3), 289–294. <https://doi.org/10.1007/s00217-003-0850-9>
- Xu, M. (2024). *Research on remaining useful life prediction methods of rolling bearings based on deep transfer learning [Master's thesis]*. Xidian University. <https://kns.cnki.net/KCMS/detail/detail.aspx?dbcode=CMFD&dbname=CMFDTEMP&filename=1025241900.nh>.
- Xu, W., Cheng, L., Lei, S., Yu, L., & Jiao, W. (2024). Mixed-flow pump cavitation characteristics extraction based on power spectrum density through pressure pulsation signal analysis. *Mechanical Systems and Signal Processing*, 208, Article 110904. <https://doi.org/10.1016/j.ymssp.2023.110904>
- Xu, H., Zhang, J., Jiang, X., & Song, C. (2025). Driver behavior recognition method via MobileViT model and optical flow fusion. *Automotive Engineering*, 47(8), 1479–1489. <https://doi.org/10.19562/j.chinasae.qcgc.2025.08.005>
- Yu, D., Li, K., Yu, S., Trinh, H., Zhang, P., Oo, A. M. T., & Hu, Y. (2021). A novel power and signal composite modulation approach to powerline data communication for SRM in distributed power grids. *IEEE Transactions on Power Electronics*, 36(9), 10436–10446. <https://doi.org/10.1109/TPEL.2021.3061469>
- Zhang, G., Fu, Q., Fu, Z., Li, X., Matetić, M., Brkic Bakaric, M., & Jemrić, T. (2020). A comprehensive peach fruit quality evaluation method for grading and consumption. *Applied Sciences*, 10(4), 1348. <https://doi.org/10.3390/app10041348>
- Zhang, W., Lv, Z., Shi, B., Xu, Z., & Zhang, L. (2021). Evaluation of quality changes and elasticity index of kiwifruit in shelf life by a nondestructive acoustic vibration method. *Postharvest Biology and Technology*, 173, Article 111398. <https://doi.org/10.1016/j.jpostharvbio.2020.111398>
- Zhang, W., Lv, Z., & Xiong, S. (2018). Nondestructive quality evaluation of agro-products using acoustic vibration methods—A review. *Critical Reviews in Food Science and Nutrition*, 58(14), 2386–2397. <https://doi.org/10.1080/10408398.2017.1324830>
- Zhuang, F., Qi, Z., Duan, K., Xi, D., Zhu, Y., Zhu, H., Xiong, H., & He, Q. (2021). A comprehensive survey on transfer learning. *Proceedings of the IEEE*, 109(1), 43–76. <https://doi.org/10.1109/JPROC.2020.3004555>
- Zulkifli, N., Hashim, N., Harith, H. H., & Mohamad Shukery, M. F. (2020). Finite element modelling for fruit stress analysis—A review. *Trends in Food Science & Technology*, 97, 29–37. <https://doi.org/10.1016/j.tifs.2019.12.029>